

## Dip-coater revolver machine for layer processing on metallic substrates Máquina dip-coater revólver para procesamiento de recubrimientos de materiales en sustratos metálicos

J. Serrano-Pérez <sup>a,b\*</sup>, I. Pacheco-Chávez <sup>c</sup>, M. A. Camacho-González <sup>d</sup>, O. Serrano-Pérez <sup>e</sup>, J. Pacheco-Martínez <sup>c</sup>

<sup>a</sup> División de Mecatrónica, Universidad Politécnica del Valle de México, Av. Mexiquense, esq. Av. Universidad Politécnica s/n, Los Portales, 54910 Fuentes del Valle, Méx.

<sup>b</sup> Colegio de Estudios Científicos y Tecnológicos del Estado de México Plantel Tultepec, Calle 16 Nte s/n, Unidad CTM, 54985, Santiago Teyahualco, México

<sup>c</sup> Unidad de Estudios de Posgrado ESIME Azcapotzalco, Instituto Politécnico Nacional, Calz. Azcapotzalco - La Villa, El Jaguey, Azcapotzalco, 02519 Ciudad de México, CDMX.

<sup>d</sup> División de Nanotecnología, Universidad Tecnológica de Tecámac, Carretera Federal México - Pachuca Km 37.5, CP 55740, Col. Sierra Hermosa, Tecámac, Estado de, 55740 San Martín Azcatepec, Méx.

<sup>e</sup> Unidad Profesional Interdisciplinaria de Ingeniería Campus Guanajuato, Instituto Politécnico Nacional, Guanajuato 36275, México

### Abstract

This work presents the design and construction of a dip-coater revolver machine to manufacture homogeneous coatings on metallic substrates. The material used for the fabrication of the machine structure was 6061-T6 aluminum. A Nema 23 stepper motor of 4.2 A and 24 V with a speed reducer with a 10:1 ratio that can provide an angular velocity  $\omega$  between 1-80 rpm was used for the motion system. DC linear actuator was used for the immersion process, which operates in the range of 12-24 V at 7 A, with a stroke length of 50 mm and a maximum linear speed of 12 mm/s. For the coating tests, SayerLack® black and white base paint was used on 6061-T6 aluminum substrates and 304 stainless steel substrates. Finally, the mathematical model and the simulation of an automatic PID control system were carried out to automate the coating manufacturing process.

Keywords: Dip-coating, revolver, Nema 23, PID, nanomaterials.

### Resumen

En este trabajo se presenta el diseño y construcción de una máquina dip-coater revólver utilizado para fabricar recubrimientos homogéneos en sustratos metálicos. El material utilizado para la fabricación de la estructura de la máquina fue aluminio 6061-T6, para el sistema de movimiento se utilizó un motor a pasos Nema 23 de 4.2 A y 24 V con un reductor de velocidad con una relación 10:1 que puede proporcionar una velocidad angular  $\omega$  entre 1-80 rpm. Para el proceso de inmersión se utilizó un actuador lineal de corriente directa (CD) que opera en un rango de 12-24 V a 7 A, la longitud de carrera es 50 mm y velocidad lineal máxima de 12 mm/s. Para las pruebas de recubrimientos se utilizó pintura base SayerLack® color blanco y negro en sustratos de aluminio 6061-T6 y sustratos de acero inoxidable 304. Finalmente se realizó el modelo matemático y la simulación de un sistema de control automático PID con el cual se automatizará el proceso de fabricación de recubrimientos.

Palabras Clave: Dip-coating, revólver, Nema 23, PID, nanomateriales.

### Introduction

Dip coating is one of the most widely used processes in the automotive, aerospace, marine, and other industries. Many parts must be manufactured to the highest possible quality standards.

Precise coating increases the longevity of parts by protecting them from the extreme elements that can cause rust and corrosion. One of the chemical techniques used to produce a solid material that can be used as a surface coating is the sol-gel technique (Brinker, Frye, Hurd, & Ashley, 1991). This

solid material can be synthesized in the form of ceramic crystals, microspheres, or nanospheres that can be used to improve the physical properties of a surface (Mahadik et al., 2013).

The materials used in advanced technological applications operate in different environmental conditions, exposed to corrosion, high and low temperatures, pressure, etc., which affect their structure, causing deterioration and failure of the material under static and dynamic stress conditions.

Therefore, a possible solution to avoid the degradation of the material is the use of coatings of ceramic and composite

\*Autor para la correspondencia: javier.serranoperez@cecycem.mx

Correo electrónico: ipachecoc2010@alumno.ipn.mx (Inocencia Pacheco-Chávez), acamachog@uttecamac.edu.mx (Mónica Araceli Camacho-González), oserranop@ipn.mx (Omar Serrano-Pérez), jpachecoma@ipn.mx (Jaime Pacheco-Martínez).

materials that allow an increase in corrosion resistance so that its study and experiments turn out to be very interesting for the scientific community (Agour, Hassan, El-Ainin, Khalaf, & Abdal, 2021).

The performance of sol-gel films is highly dependent on their porosity and structural quality, and it is often argued that the presence of cracks and pores degrades their properties and, consequently, their protective effectiveness (Zheludkevich, Salvador, & Ferreira, 2005).

Typically, manufacturing defects that impact coating performance stem from mechanical failures, human error, or anomalies in raw materials. Industrial processes tend to be repetitive and require fine-tuned control of various parameters to ensure consistent physical and chemical properties across all products.

Controlling parameters at different manufacturing stages is crucial. For instance, in immersion coatings, the thickness of the coating should be managed, taking into account factors such as solution properties, viscosity, and density to create a material layer successfully. Additionally, the speed of sample extraction, temperature, duration of stay, and evaporation rate must be considered. All of these factors significantly influence achieving the desired outcome: producing a uniform coating without any surface imperfections.

To minimize manufacturing errors in repetitive processes, automatic control systems are employed in machines. These systems are featured in various dip-coating machines, both commercial and prototype, equipped with open-loop and closed-loop controls. Many of these machines perform fundamental tasks necessary for the production of coatings. However, the coatings may sometimes possess different properties since specific machines are operated manually or semi-automatically. Consequently, the quality of the final coating is entirely contingent on the operator's skill. Programmable coating equipment can sometimes be prohibitively expensive and inadequately designed to meet specific industry and research laboratory needs (Dunlap et al., 2022).

Several studies suggest that designing prototypes of dip-coating machines (Ayturan, Ayturan, Dalkılıç, & Dursun, 2019; Buapool, Thavarungkul, Srisukhumbowornchai, & Termsuksawad, 2017; Castillo-Vilcatoma, Loarte, Fernandez-Chillce, Pastrana, & Pastrana, 2021) with recycled materials could potentially decrease their cost. It is noteworthy that reducing costs could positively impact the accessibility and adoption of these machines. The Arduino microcontroller plays a crucial role in controlling the process. A constant and controlled speed is maintained by providing signals to activate and deactivate a stepper motor, which in turn controls the immersion and extraction of substrate.

That is why we developed the prototype. Through the mathematical model, we can design a control algorithm and implement a PID controller in a microprocessor like Arduino. Generally, an Arduino microcontroller performs functions to maintain specific process variables within desired limits. Utilizing a PID control algorithm on an Arduino microcontroller becomes a valuable instrument for assessing the output signal and making essential adjustments in response to process disturbances.

This machine can reduce manufacturing time for layers and multilayers on diverse metallic or ceramic substrates. Additionally, it enables various coating materials due to its in-

device drying function that significantly reduces the multilayer production time. The construction of the prototype will enable assessing whether mechanical vibrations impact the quality of the film manufacturing process. By improving control over response time, response precision will increase, and most significantly, the use of PID control aids in minimizing errors and measuring disturbances. Consequently, if disturbances emerge throughout the process, rectifying them promptly and accurately is possible.

## 1. Experimental

### 1.1. 3D design, Finite Element Modeling and Materials

The traditional dip coating procedure (Figure 1) involves four fundamental stages: a) immersing the substrate at a constant pace, b) leaving the substrate in the solution, c) removing the substrate at a fixed pace, and d) evaporating the solvents.

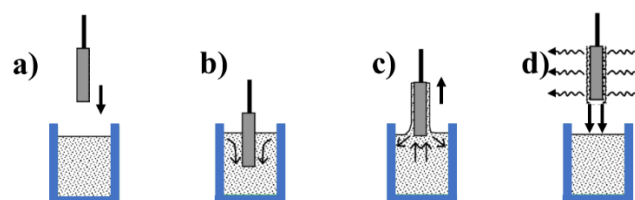


Figure 1. Dip-coating process, a) immersion, b) permanence of substrate, c) extraction and d) evaporation

Commercial dip-coaters conclude the manufacturing process during the evaporation stage. Subsequently, the substrate is extracted and transferred to a heating chamber to remove any remaining liquid elements. Heat treatment is often applied to alter the characteristics of the materials utilized as coatings.

Forming a single coating layer on a metal or ceramic substrate becomes more complex as human intervention is needed for the drying and heat treatment. The longer the manufacturing time, the higher the costs, making it expensive to produce coatings with conventional machines, especially if multiple layers are required.

Different robot prototypes and control systems exist in industrial robotics, providing practical solutions for industrial manufacturing processes. (Aguilar-Ibanez et al., 2022; García-Sánchez et al., 2020; Meda-Campaña et al., 2022; Rubio, 2016, 2017; Rubio, Cruz, et al., 2016; Rubio et al., 2019; Rubio, Hernández-Aguilar, Ávila-Camacho, Stein-Carrillo, & Meléndez-Ramírez, 2016; Rubio, Pacheco, Pérez-Cruz, & Torres, 2012; Rubio, Torres, & Aguilar, 2011; Serrano-Pérez, G. Villarreal-Cervantes, Rodríguez-Molina, & Serrano-Pérez, 2021; Torres, Rubio, Aguilar-Ibañez, & Pérez-Cruz, 2012; Villarreal-Cervantes, Serrano-Pérez, & Rodríguez-Molina, 2021).

The project builds upon the design of an articulated robotic arm as a basis for the dip-coating process. This design offers necessary features for reducing time and movement in the coating manufacturing process. The 3D design of the dip-coating revolver prototype, made in SolidWorks®, is presented in Figure 2.

This equipment includes a primary axis (link 1) capable of angular movement from 0 to 360°. Link 1 includes a cantilever

beam structure that supports a linear actuator on each end. Each linear actuator can move up to 50 mm linearly. Link 1's load is supported by a bearing attached to an aluminum plate, which creates a rigid structure that prevents deflection during operation. The bottom segment of link one is connected to a Nema 23 worm gearbox stepper motor that initiates the motion of link 1.

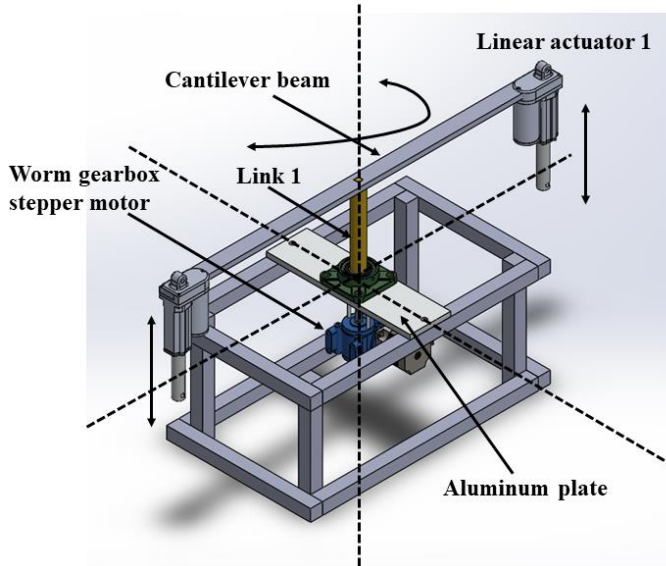


Figure 2. Dip-coating revolver prototype modelling in SolidWorks®

For this prototype, it is essential to conduct a structural analysis of the element exposed to the static load due to the weight of Link 1 and its components. This analysis is necessary to ensure the design is sufficient for equipment safety during handling. Figure 3 depicts the system in which the total load  $W_T$  is applied to the structure. Table 1 lists the weights of the various elements that comprise the prototype.

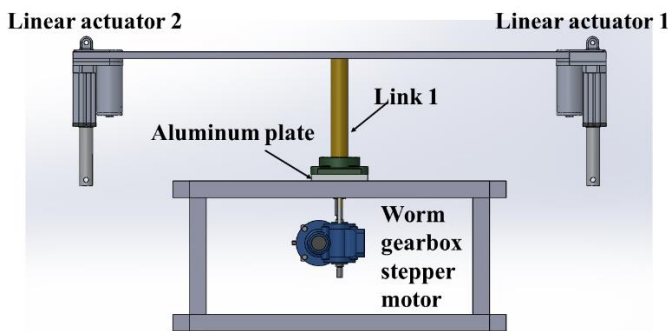


Figure 3. Scheme for the structural analysis of the prototype dip-coating revolver

Table 1. Weight of prototype components

|   | W (kg) |
|---|--------|
| Cylindrical bar (link 1, 30 cm x 3.14 cm <sup>2</sup> )   | 0.604  |
| Aluminum profile (cantilever beam 108.5 cm x 4 cm x 2 cm) | 2.095  |
| Pneumatic linear actuator 1                               | 1.347  |
| Pneumatic linear actuator 2                               | 1.347  |
| Bearing   | 0.592  |
| Worm gearbox stepper motor                                | 2.794  |

Based on Table 1, the total load ( $W_T$ ) can be calculated as 8.779 kg, equivalent to 86.12 N. Using equation (1), we can calculate the deflection  $y_{max}$  in the structure and ensure the prototype operates safely with the finite element method in SolidWorks® and ANSYS® Workbench™.

$$y_{max} = -\frac{PL^3}{48EI} \quad (1)$$

The model was created based on the dimensions displayed in Figure 4a to conduct a finite element method analysis. The mechanical properties of Aluminum 1060, including a modulus of elasticity of  $E=69,000$  MPa, a Poisson's ratio of 0.33, and a density of  $2700 \text{ kg/m}^3$ , were subsequently considered for static analysis. In this instance, the beam is supported by two simple supports. The ANSYS Workbench program applies fixed support restrictions to the surfaces where the fastening screws need placement. A -86.12 N force is also introduced, as depicted in Figure 4b. The beam meshing was performed using an element size of 0.005 m.

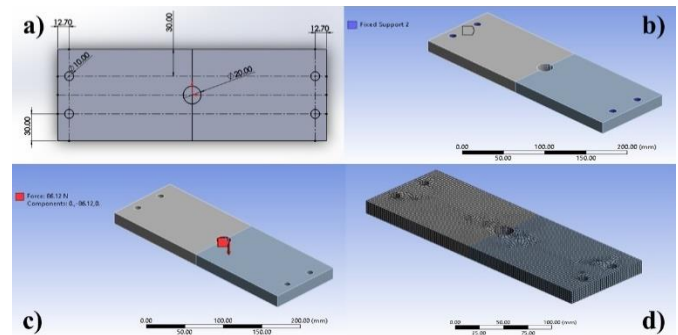


Figure 4. Aluminum plate ANSYS® Workbench™ Simulation

## 2.2 Open Loop Control System

Industrial processes typically use open-loop or closed-loop automatic control systems for repetitive tasks. In many cases, open-loop automatic control systems lack a measurement system to evaluate output values, or they may exist but not influence input values. The parameters in open control systems are usually regulated based on experimentation or previous measurements. For the mechanical drive, a 4.2 A Nema 23 motor was utilized. This is a 1.8° degree bipolar hybrid stepper motor commonly used in small to medium-power CNC machines. Table 2 displays the primary specifications of the Nema 23 stepper motor.

Table 2. Characteristics of the Nema 23 stepper motor

| Type                 | NEMA 23            |
|----------------------|--------------------|
| Step angle           | 1.8 degrees        |
| Steps per lap        | 200                |
| Current              | 4.2 A/phase        |
| Holding torque       | 18 Kg-cm (1.8 N.m) |
| Number of phases     | 2                  |
| Number of conductors | 4                  |
| Arrow diameter       | 8 mm               |

The DM542T stepper motor driver controls the stepper motor speed and direction. It accepts an input voltage ranging from 9V to 42V and can withstand peak currents of up to 4A, which is sufficient for most commercial stepper motors. Refer to Table 3 for the main specifications of the stepper motor driver.

Table 3. Stepper motor controller features

|                       |                           |
|-----------------------|---------------------------|
| Input current         | 0 to 4A                   |
| Input voltage         | 9 to 42V                  |
| Current output        | 0.5 to 4A                 |
| Control signals       | 3.3 to 24V                |
| Maximum power         | 160W                      |
| Operating temperature | -10 to 45 °C              |
| Micro Step            | 1, 2/A, 2/B, 4, 8, 16, 32 |

Finally, we utilized the mks-osc V1.0 PWM stepper motor control unit, which functions as a PWM pulse generation module and allows for speed control ranging from 8-24V. This unit generates the conductive step signal. The controller offers three frequency signal options: high (5.4k-160kHz), medium (540-16.6kHz), and low (80-2.4kHz), which can be adjusted for speed by jumper selection.

The various elements of the open-loop control system enable the necessary parameter adjustments for manufacturing coatings with various materials, including monolayer and multilayer coatings, and utilizing different substrate types, such as metallic and ceramic materials. Based on the experimental findings, it is feasible to implement an automatic control system to conduct repetitive manufacturing processes with improved quality, time efficiency, and cost-effectiveness. Therefore, obtaining a mathematical model of the machine is essential to implement the automatic control system. Figure 5 depicts the schematic diagram of the mechanical system's connections and the control in an open loop.

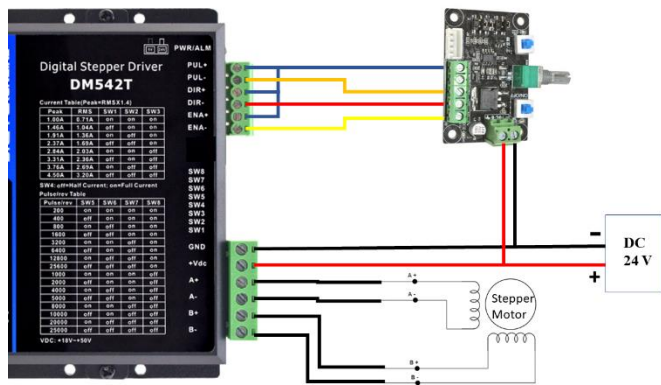


Figure 5. Open loop control system of the revolver dip-coating machine

### 2.3 Mathematical model of the dip-coating revolver machine

The mathematical model comprises one equation representing the electrical components and one for the mechanical counterparts. Figure 6 depicts the schematic diagram of the electromechanical system employed in the revolver dip-coating equipment. The voltage  $v(t)$  is related to

resistance and inductance  $L \frac{di(t)}{dt}$  through equation (2) for the analysis of the electrical circuit mesh.

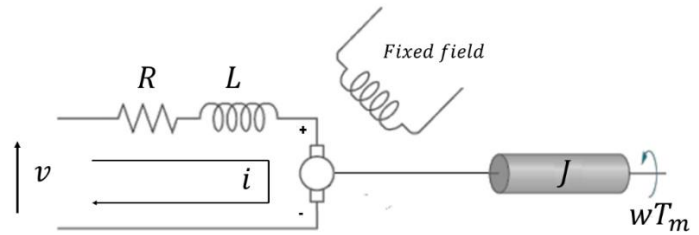


Figure 6. Schematic diagram of electromechanical system of the prototype

$$v(t) = Ri(t) + L \frac{di(t)}{dt} + E_a(t) \quad (2)$$

The first equation of the circuit (3) is obtained by removing the  $L \frac{di(t)}{dt}$  term from the previous equation.

$$L \frac{di(t)}{dt} = v(t) - Ri(t) - E_a(t) \quad (3)$$

The equation models the mechanical system (4) below, where  $T_m(t)$  represents the motor torque,  $B$  is the equivalent friction coefficient for the motor and shaft load,  $J$  is the moment of inertia, and  $w(t)$  denotes the angular velocity.

$$T_m(t) = J \frac{dw(t)}{dt} + Bw(t) \quad (4)$$

From equation 4, we obtained the second differential equation representing the dynamic system (5).

$$J \frac{dw(t)}{dt} = T_m(t) - Bw(t) \quad (5)$$

Equation (6) calculates the back electromotive force  $E_a(t)$  by utilizing  $K_a$ , a constant that proportionally relates  $v(t)$  to  $w(t)$ .

$$E_a(t) = K_a w(t) \quad (6)$$

The equation (7) can be used to calculate  $T_m(t)$ , with a mechanical relationship establishing that  $T_m(t)$  is proportional to the electric current  $i(t)$ .

$$T_m(t) = K_m i(t) \quad (7)$$

By solving differential equations (3), (5), (6), and (7), and applying the Laplace transform, we obtain equations (8), (9), (10), and (11).

$$Lsi(s) = v(s) - Ri(s) - E_a(s) \quad (8)$$

$$Jsw(s) = T_m(s) - Bw(s) \quad (9)$$

$$E_a(s) = K_a w(s) \quad (10)$$

$$T_m(s) = K_m i(s) \quad (11)$$

By replacing equations (10) and (11) into equation (8), a novel equation (12) is derived.

$$v(s) = \frac{(R + Ls)T_m(s)}{K_m} + K_a w(s) \quad (12)$$

From equation 9, we calculate  $w(t)$ , which is then substituted into equation 12 to generate a new equation 13.

$$v(s) = \frac{(R + Ls)T_m(s)}{K_m} + K_a \frac{T_m(s)}{Js + B} \quad (13)$$

This is how to derive the initial transfer function that connects  $T_m(t)$  to  $v(s)$  (14).

$$\frac{T_m(s)}{v(s)} = \frac{K_m(Js + B)}{LJs^2 + (RJ + LB)s + RB + K_m K_a} \quad (14)$$

The equation (15) provides the transfer function that connects the back emf with  $v(s)$ .

$$\frac{E_a(s)}{v(s)} = \frac{K_m K_a}{LJs^2 + (RJ + LB)s + RB + K_m K_a} \quad (15)$$

The equation (16) represents the transfer function that connects  $i(s)$  to  $v(s)$

$$\frac{i(s)}{v(s)} = \frac{Js + B}{LJs^2 + (RJ + LB)s + RB + K_m K_a} \quad (16)$$

The equation that relates  $v(t)$  to  $w(t)$  is represented by the transfer function (17).

$$\frac{w(s)}{v(s)} = \frac{K_m}{s(LJs^2 + (RJ + LB)s + RB + K_m K_a)} \quad (17)$$

Finally, equation (18) represents the transfer function that relates  $v(s)$  to the angular position  $\theta(s)$ .

$$\frac{\theta(s)}{v(s)} = \frac{K_m}{s(LJs^2 + (RJ + LB)s + RB + K_m K_a)} \quad (18)$$

To analyze the inputs and outputs of the system, the mathematical model is represented in the state space (19) of the motor by the differential equations obtained in the

mathematical model. In this case  $x_1 = w$  is the  $w(t)$ ,  $\dot{x}_1 = \dot{w}$  is the angular acceleration,  $x_2 = i$  the armature current and  $\dot{x}_2 = \dot{i}$  the  $v(t)$ .

$$\begin{aligned} \dot{x}_1 &= -\frac{B}{J}x_1 + \frac{K_m}{J}x_2 \\ \dot{x}_2 &= -\frac{R}{L}x_2 - \frac{K_a}{L}x_1 + \frac{1}{L}v \end{aligned} \quad (19)$$

Finally, the state space representation is (20).

$$\begin{aligned} \begin{bmatrix} \dot{x}_1 \\ \dot{x}_2 \end{bmatrix} &= \begin{bmatrix} -\frac{B}{J} & \frac{K_m}{J} \\ -\frac{K_a}{J} & -\frac{R}{L} \end{bmatrix} \begin{bmatrix} x_1 \\ x_2 \end{bmatrix} + \begin{bmatrix} 0 \\ \frac{1}{L} \end{bmatrix} v \\ \begin{bmatrix} y_1 \\ y_2 \end{bmatrix} &= \begin{bmatrix} 1 & 0 \\ 0 & 1 \end{bmatrix} \begin{bmatrix} x_1 \\ x_2 \end{bmatrix} \end{aligned} \quad (20)$$

### 2.3. PID Controller Design

A PID controller is a device that allows a system to be controlled to achieve a desired output state. It consists of three elements: proportional, integral, and derivative. The transfer function that defines the proportional, integral, and derivative parts can be seen in equation (21).

$$G_c(s) = K_p \left( 1 + \frac{1}{t_i s} + t_d s \right) \quad (21)$$

The controller output  $u(t)$  is given by equation 22 when the error signal  $e(t)$  is input to the controller.

$$u(t) = K_p \left[ e(t) + \frac{1}{t_i} \int_0^t e(t) dt + t_d \frac{de(t)}{dt} \right] \quad (22)$$

Equation (20) can be reduced to an equation based on the proportional gain ( $K_p$ ), the integral gain ( $K_i$ ) and the derivative gain ( $K_d$ ), obtaining equation (23).

$$G_c(s) = K_p + \frac{K_i}{s} + K_d s \quad (23)$$

Through the transfer function equation (17), which relates the  $w(t)$  to the  $v(s)$ , it is possible to observe a sigmoidal-type graph. The parameters used for this transfer function are given in Table 4.

|                         |                             |
|-------------------------|-----------------------------|
| Moment of inertia       | $J = 0.0658 \text{ kg m}^2$ |
| Input voltage           | 24V                         |
| Rated current           | 4.2A                        |
| Armature resistance     | $R = 1.4 \Omega$            |
| Armature inductance     | $L = 0.0068 \text{ H}$      |
| Coefficient of friction | $B = 1.9 \text{ Nm}$        |

|                  |                      |
|------------------|----------------------|
| Angular velocity | $w = 60 \text{ rpm}$ |
|------------------|----------------------|

By substituting the numerical values of the parameters in equation (24) it is possible to obtain the transfer function that describes the dynamics of the system.

$$\frac{w(s)}{v(s)} = \frac{0.96}{0.000447s^2 + 0.105s + 3.58} \quad (24)$$

To approximate the dynamics of the process, a first-order transfer function was used with two constants, the delay L and the time constant, as shown in equation (24). The gain K of equation (25) is the value at which the system stabilizes and is determined according to the Ziegler-Nichols method.

$$G_p s = \frac{Ke^{-Ls}}{ts + 1} \quad (25)$$

As a result of the adjustment of the dynamic approximation, the constants  $K = 6.44$ ,  $L = 0.00712$  and  $ts = 0.03125$  were obtained. The next part of the method is to design the proportional, integral, and derivative control using the previously calculated constants. Table (5) shows the design of the control system.

Table 5. P, PI and PID control constants

| Control | $K_p$  | $t_i$  | $t_d$  |
|---------|--------|--------|--------|
| P       | 0.6815 | 0      | 0      |
| PI      | 0.6133 | 0.0237 | 0      |
| PID     | 0.8178 | 0.0142 | 0.0035 |

#### 2.4. Coating materials

Commercially available 6061-T6 aluminum sheets (Figure 7a) and 304 stainless steel sheets (Figure 7b) were used to fabricate the metal substrates. The dimensions of the substrates are 100 mm x 10 mm x 3.18 mm. The liquid solution used for the coating is a commercially available SayerLack® brand high corrosion resistance metal enamel used to prevent rust from appearing on metal surfaces.

The following parameters were used for the coatings: a) immersion at a speed of 3 mm/s, b) residence time in the solution of 20 s, c) extraction speed of 3 mm/s, and d) drying time of 10 min. This procedure was performed four times on each sample, alternating black and white inks.

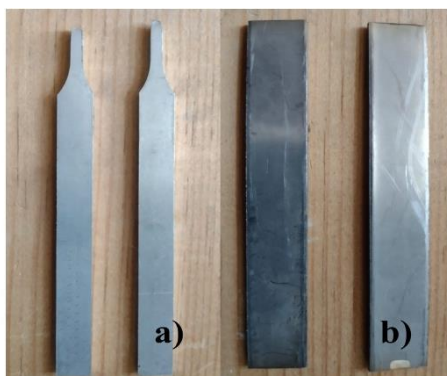


Figure 7. a) Aluminum substrate, b) Stainless steel 304 substrate

## Results and discussion

### 3.1 Construction of the prototype dip-coater revolver

As specified in the design, the prototype was built using off-the-shelf materials resistant to environmental factors such as moisture. Figure 8 shows the prototype of the Dip Coater Revolver, which works with a stepper motor coupled to a reduction gear controlled by a Nema 23; in addition, a linear actuator has been coupled to perform the immersion and extraction process with speed control, so that with this device it is possible to produce layers and multilayers with the same characteristics since the time and speed control parameters remain constant from one coating to another.

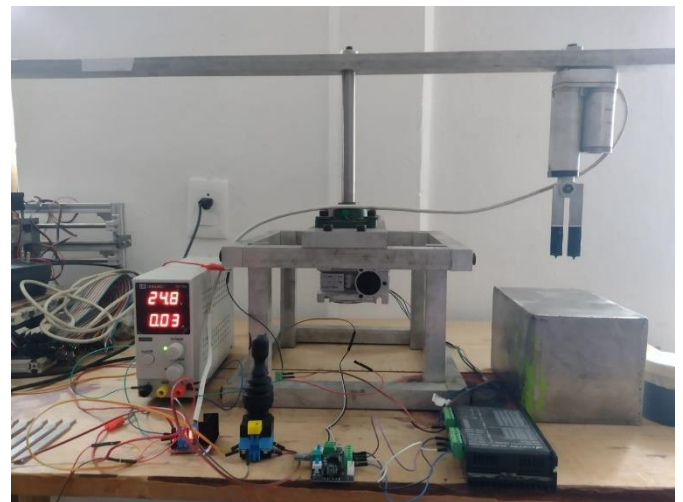


Figure 8. Schematic diagram of electromechanical system of the prototype

### 3.2. Finite Element Modeling

The  $y_{max}$  analysis was carried out on the main beam of the prototype since this is the structural element that is mainly subjected to static and dynamic loads. In order to guarantee a good design and choice of material for the construction, it is necessary to satisfy that the maximum allowable  $y_{adm}$  must be  $L/180$ , where L is the length of the beam. In this case, the L is 300 mm. According to the design condition, the maximum allowable  $y_{max}$  for this beam will be 1.66 mm. The numerical simulation performed in ANSYS Workbench (Figure 9) results in a  $y_{max}$  of 0.0106 mm, which is lower than the value of  $y_{adm}$ .

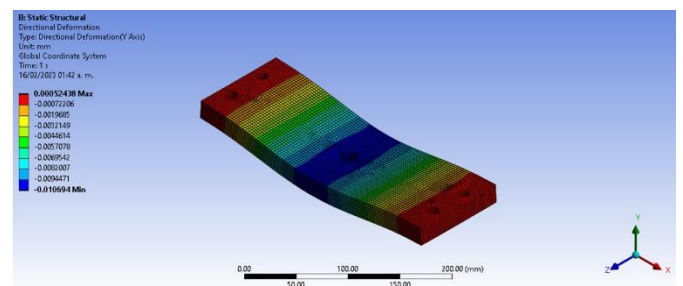


Figure 9. Numerical analysis of the beam in ANSYS® Workbench™

The design and analysis of the structure ensure that the equipment can be operated safely and that there are no inertia problems due to the static and mobile charges required to produce a coating.

### 3.3. PID control

In order to validate the dynamic model, the numerical simulation was performed in Simulink®. The results of the simulation and experimentation are shown in Figure 10.

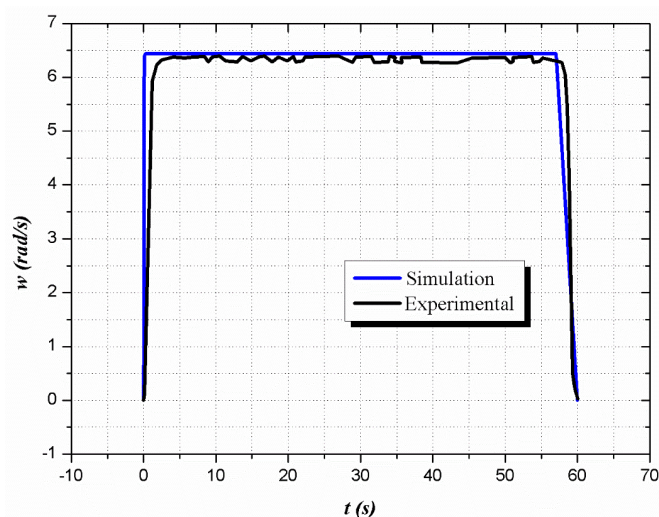


Figure 10. PID dynamic model experimental and simulation

With the parameters of the stepper motor established, it can be seen that the system reacts quickly when running. With these data, it is possible to design a control law for the system that will allow the automation of the coating production process depending on the type of substrates (metallic, ceramic, composite), making a reproducible process, i.e., all coatings will have very similar characteristics between them (film thickness, optical properties, etc.).

### 3.4. Coatings

It was observed that the coatings made with enamel metal paint have a uniform appearance (Figure 11), no defects are observed on its surface, and the process of making four layers of black and white coatings took about 43 minutes.

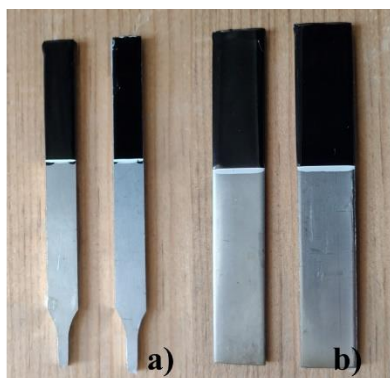


Figure 11. a) Aluminum coating, b) Stainless steel coating

In addition, it is worth mentioning that with this tool, it is possible to make reproducible coatings, i.e., it is possible to make coatings with the same properties because the process is semi-automatic by the machine.

## 2. Conclusion

The purpose of manufacturing the Dip Coater Revolving Machine is to use a flexible tool to produce thin coatings and nanofilms, as many industrial and research processes currently require this technique. With this device, the production of thin coatings and nanofilms is faster, directly leading to a reduction in time and, therefore, cost.

The analysis of the aluminum plate, which supports all the moving elements of the prototype, allows us to determine a  $y_{max}$  of 0.0106 mm, which guarantees that the equipment will not be subjected to excessive stress during the coating process.

An excellent approximation was observed between the simulated PID and experimental dynamic models. This mathematical model will allow the generation of a control algorithm to be implemented in an ARDUINO microcontroller to monitor the operating variables during the manufacturing process.

Multilayer production time has been significantly reduced. In initial trials, a 4-layer coating was completed in approximately 43 minutes. The traditional process took approximately 2 hours to complete.

Future work will implement a drying system in the prototype to further reduce the production time of thin multilayers.

## Funding

The authors acknowledge the support of the Secretaría de Investigación y Posgrado (SIP-IPN) [Grant SIP-20230156].

## 3. References

- Agour, M. A. E., Hassan, M. K., El-Ainin, H. A., Khalaf, M. S., & Abdal, A. (2021). Sol-Gel/Dip Coating Technique for corrosion protection of petroleum pipeline steel. *Journal of Advanced Engineering Trends*, 40(1), 129-134. doi:10.21608/jaet.2021.82252
- Aguilar-Ibanez, C., Jimenez-Lizarraga, M. A., Gandarilla-Esparza, I., Moreno-Valenzuela, J., Saldivar, B., Suarez-Castanon, M. S., & Rubio, J. J. (2022). Robust Velocity and Load Observer for a General Noisy Rotating Machine. *Machines*, 10(11), 1009. doi:https://doi.org/10.3390/machines10111009
- Ayturan, Z. C., Ayturan, Y. A., Dalkılıç, E., & Dursun, Ş. (2019). Homemade dip coating machine for thin films. *International Symposium for Environmental Science and Engineering Research*.
- Brinker, C. J., Frye, G. C., Hurd, A. J., & Ashley, C. S. (1991). Fundamentals of sol-gel dip coating. *Thin Solid Films*, 201(1), 97-108. doi:https://doi.org/10.1016/0040-6090(91)90158-T
- Buapool, S., Thavarungkul, N., Srisukhumbowornchai, N., & Termsuksawad, P. (2017). Modeling and Analysis of the Effect of Dip-Spin Coating Process Parameters on Coating Thickness Using Factorial Design Method. *Hindaw Advances in Materials Science and Engineering*, 1-10. doi:https://doi.org/10.1155/2017/9639306
- Castillo-Vilcatoma, D. A., Loarte, S. J., Fernandez-Chillcce, A. A., Pastrana, E. C., & Pastrana, R. Y. (2021). Designing and fabrication of a low-cost

- dip-coater for rapid production of uniform thin films. *Química Nova*, XY(00), 1-4. doi:10.21577/0100-4042.20170805
- Dunlap, C., Featherstone, S., Smith, M., Vu, M., Williams, A., Bailey, J., & Hu, H. (2022). Design and fabrication of a low-cost and programmable dip coating machine. *HardwareX*, 12, 1-23. doi:https://doi.org/10.1016/j.ohx.2022.e00364
- García-Sánchez, J. R., Tavera-Mosqueda, S., Silva-Ortigoza, R., Hernández-Guzmán, V. M., Marciano-Melchor, M., Rubio, J. J., . . . Martínez-Martínez, J. (2020). A Novel Dynamic Three-Level Tracking Controller for Mobile Robots Considering Actuators and Power Stage Subsystems: Experimental Assessment. *Sensors*, 20(17), 1-25. doi:https://doi.org/10.3390/s20174959
- Mahadik, S. A., Parale, V. G., Vhatkar, R. S., Mahadik, D. B., Kavale, M. S., Wagh, P. B., . . . Gurav, J. L. (2013). Superhydrophobic silica coating by dip coating method. *Applied Surface Science*, 277, 67-72. doi:https://doi.org/10.1016/j.apsusc.2013.04.001
- Meda-Campaña, J. A., Rodríguez-Manzanarez, R. A., Ontiveros-Paredes, S. D., Rubio, J. J., Tapia-Herrera, R., Cortés, T. H., . . . Aguilar-Ibáñez, C. (2022). An Algebraic Fuzzy Pole Placement Approach to Stabilize Nonlinear Mechanical Systems. *IEEE Transactions on Fuzzy Systems*, 30(8), 3322-3332. doi:10.1109/TFUZZ.2021.3113560
- Rubio, J. J. (2016). Interpolation neural network model of a manufactured wind turbine. *Neural Computing and Applications*, 28, 2017–2028. doi:https://doi.org/10.1007/s00521-015-2169-4
- Rubio, J. J. (2017). A method with neural networks for the classification of fruits and vegetables. *Soft Computing*, 21, 7207–7220 doi:DOI 10.1007/s00500-016-2263-2
- Rubio, J. J., Cruz, P., Paramo, L. A., Meda, J. A., Mujica, D., & Ortigoza, R. S. (2016). PID Anti-Vibration Control of a Robotic Arm. *IEEE Latin America Transactions*, 14(7), 3144 - 3150. doi:10.1109/TLA.2016.7587614
- Rubio, J. J., García, E., Aquino, G., Aguilar-Ibáñez, C., Pacheco, J., Meda-Campaña, J. A., & C.J.Brinker. (2019). Mínimos Cuadrados Recursivos para un Manipulador que Aprende por Demostración. *Revista Iberoamericana de Automática e Informática Industrial*, 16, 147-158. doi:https://doi.org/10.4995/riai.2019.8899
- Rubio, J. J., Hernández-Aguilar, J. A., Ávila-Camacho, F. J., Stein-Carrillo, J. M., & Meléndez-Ramírez, A. (2016). Sistema sensor para el monitoreo ambiental basado en redes Neuronales. *Ingeniería Investigación y Tecnología*, XVII(2), 211-222.
- Rubio, J. J., Pacheco, J., Pérez-Cruz, J. H., & Torres, F. (2012). Mathematical model with sensor and actuator for a transelevator. *Neural Computing and Applications*, 24, 277–285. doi:https://doi.org/10.1007/s00521-012-1224-7
- Rubio, J. J., Torres, C., & Aguilar, C. (2011). Optimal control based in a mathematical model applied to robotic arms. *International Journal of Innovative Computing, Information and Control*, 7(8), 5045–5062.
- Serrano-Pérez, O., G.Villarreal-Cervantes, M., Rodríguez-Molina, A., & Serrano-Pérez, J. (2021). Offline robust tuning of the motion control for omnidirectional mobile robots. *Applied Soft Computing*, 110, 1-17. doi:https://doi.org/10.1016/j.asoc.2021.107648
- Torres, C., Rubio, J. J., Aguilar-Ibáñez, C. F., & Pérez-Cruz, J. H. (2012). Stable optimal control applied to a cylindrical robotic arm. *Neural Computing and Applications*, 24, 937–944. doi:10.1007/s00521-012-1294-6
- Villarreal-Cervantes, M. G., Serrano-Pérez, O., & Rodríguez-Molina, A. (2021). Novel Asynchronous Activation of the Bio-Inspired Adaptive Tuning in the Speed Controller: Study Case in DC Motors. *IEEE Access (Volume: 9)*, 9, 138976 - 138993. doi:10.1109/ACCESS.2021.3118658
- Zheludkevich, M. L., Salvado, I. M., & Ferreira, M. G. S. (2005). Sol-gel coatings for corrosion protection of metals. *Journal of Materials Chemistry*(48), 5099–5111 doi:https://doi.org/10.1039/B419153F